CIHAN
UNIVERSITY- ERBIL

Department of Nutrition and Dietetics
College of Health Technology

Title:

Maximum performance of neutralizing antibodies depends on Fc function

Dr. Esmat Khaleqsefat

Jan.25th, 2024

ABSTRACT

- Background: Neutralizing antibodies (NAbs): effective in treating COVID-19
- Method: bioluminescence imaging (BLI): real-time monitoring of NAb treatment
- Result: 1- virus spreads from nasal cavity to body 2- NAbs and Fc effector function require for prevention and treatment of infection 3- Monocytes, neutrophils and NK cells contribute to Fc- dependent NAb protection
- Conclusion: Fab and Fc against SARS-CoV-2.

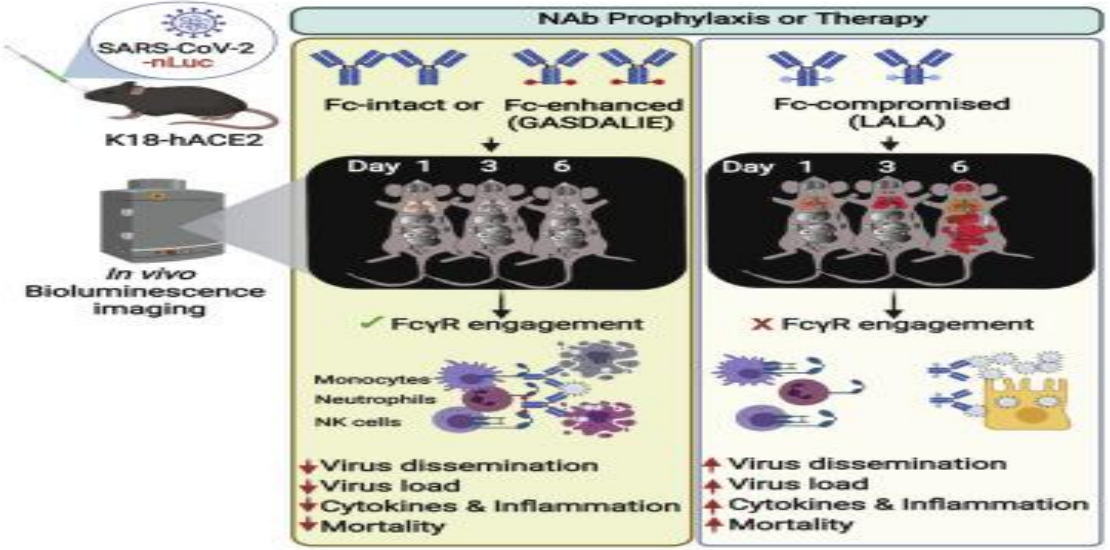

INTRODUCTION

Neutralizing monoclonal antibodies (NAbs)

- Multiple NAbs against the spike (S) glycoprotein of SARS-CoV-2
- NAbs bind to the receptor-binding domain (RBD) in S1 subunit and inhibit virus attachment to human angiotensin-converting enzyme 2 (hACE2) receptor
- NAbs showed varying levels of efficacy and protection, however, in vitro and in vivo neutralization potency of NAbs not consistently correlated

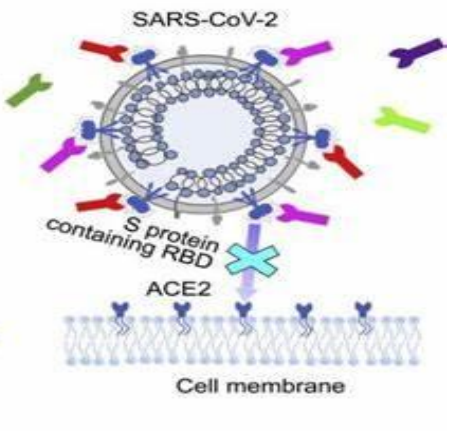

Introduction

Fc

- Antigen-binding domain (Fab) of antibodies are critical for neutralization,
- Fragment crystallizable (Fc) domain influence *in vivo* efficacy
- Fc effector functions can also be detrimental to the host, leading to antibody-dependent enhancement and aggravated disease pathology

Animal models

- Transgenic mice (K18-hACE2 mice) advantages are:

a. Heightened susceptibility to human-tropic SARS-CoV-2 virus strains

b. K18-hACE2 mice also display impaired respiratory function

c. Mouse FcγRs display similar affinities to human antibodies.

Bioluminescence imaging (BLI)

- Permit live visualization of pathogen spread in relevant tissues,
- Enabling real-time outcome assessments for treatment regimens.

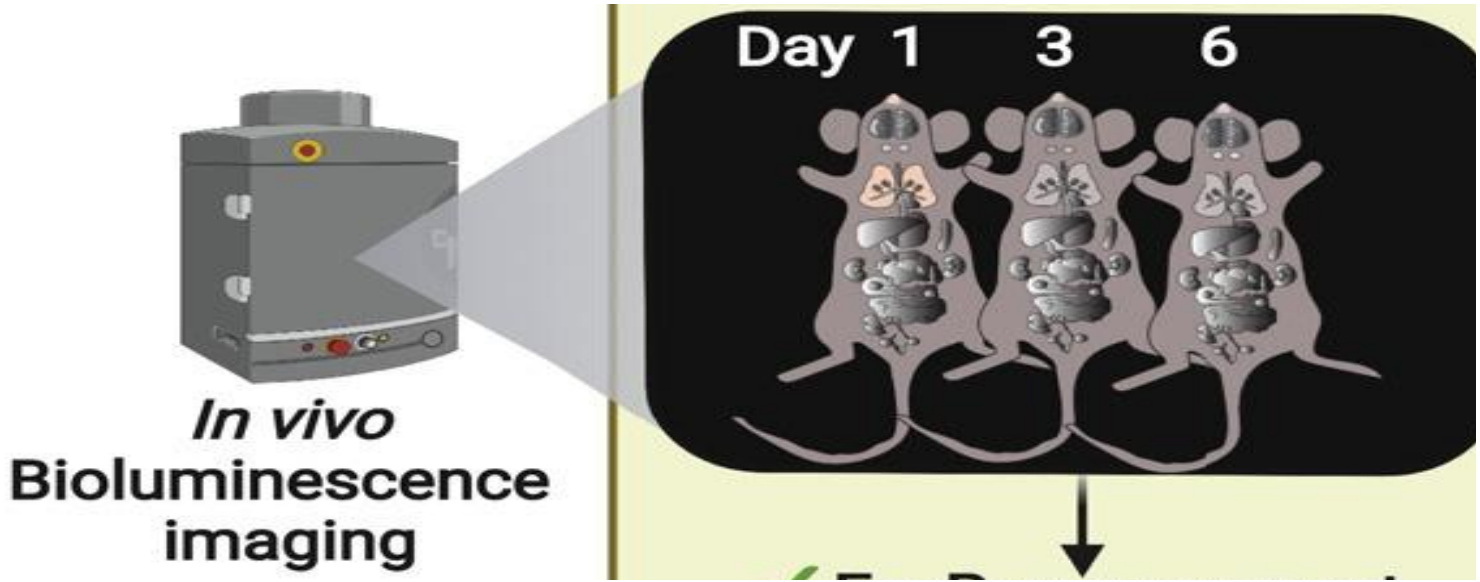

SARS-CoV-2-nLuc

- SARS-CoV-2 virus carrying a nanoluciferase (nLuc) reporter in place of ORF7A gene

I. Closely mimics wild-type virus replication kinetics
II. Stably maintains nLuc reporter over five generations in vitro
III. ORF7a deletion not to affect pathology of wild-type virus

METHODS

- ✔ Bioluminescence Imaging (BLI) of SARS-CoV-2 infection
- ✔ Protein expression and purification
- ✔ Cryo-immunohistology of organs
- ✔ Analyses of signature inflammatory cytokines mRNA expression
- ✔ Antibody depletion of immune cell subsets
- ✔ Flow Cytometric Analyses
- ✔ Electron Microscopy and Dual-Axis Tomography
- ✔ Immunoelectron microscopy
- ✔ Mutagenesis of human antibodies
- ✔ Flowcytometry analysis of cell-surface Spike staining
- ✔ Virus capture assay
- ✔ Surface plasmon resonance (SPR)
- ✔ SARS-CoV-2 MA10 neutralization assay
- ✔ Antibody dependent cellular cytotoxicity (ADCC) assay
- ✔ Antibody dependent cellular phagocytosis (ADCP) assay
- ✔ smFRET imaging of S on SARS-CoV-2 VLPs (S-MEN particles)

✔ Bioluminescence Imaging (BLI) of SARS-CoV-2 infection

Fig 1 (A)- SARS-CoV-2-carrying nLuc reporter in ORF7a for non-invasive BLI of virus spread following intranasal (i.n.) challenge of mice.

RESULTS

BLI allows visualization of SARS-CoV-2 replication dynamics and pathogenesis

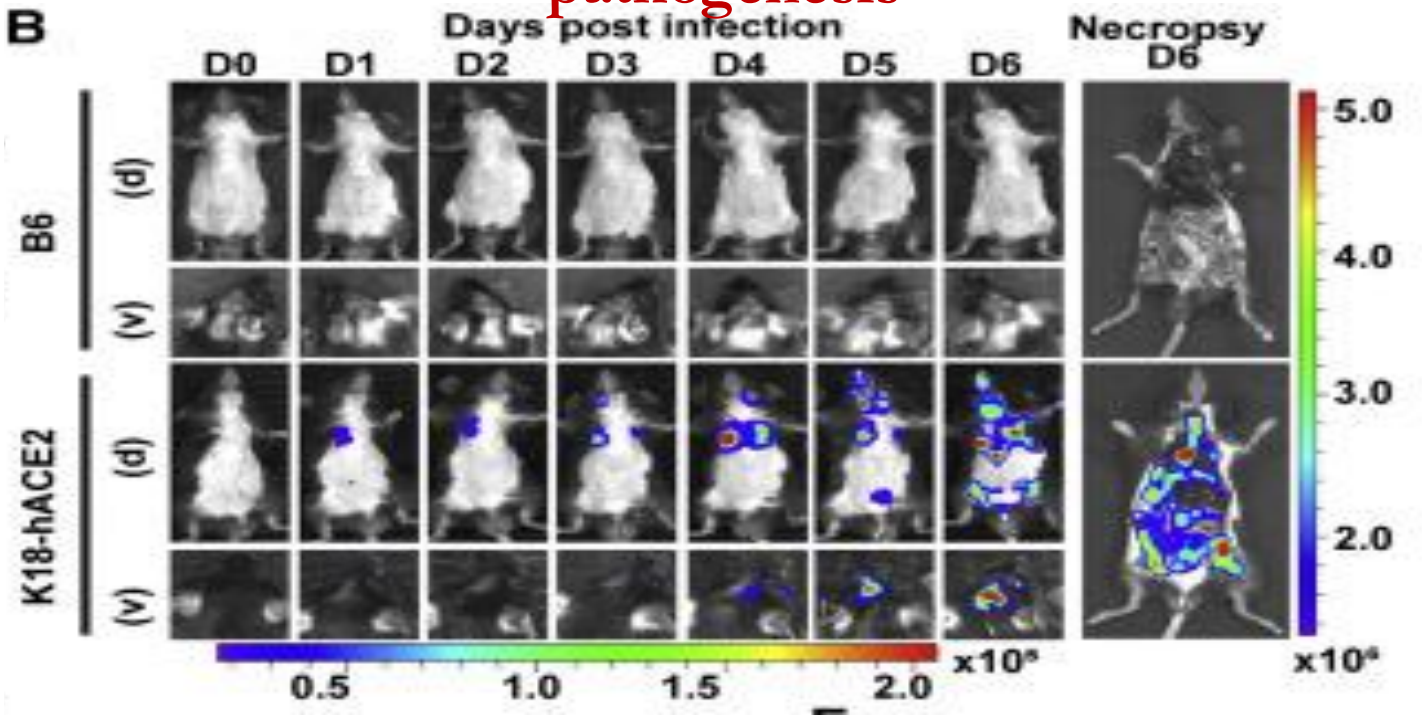

Fig 1 (B)- Representative images from temporal BLI of SARS-CoV-2-nLuc-infected mice in ventral (v) and dorsal (d) positions at the indicated dpi and after necropsy.

BLI allows visualization of SARS-CoV-2 replication dynamics and pathogenesis

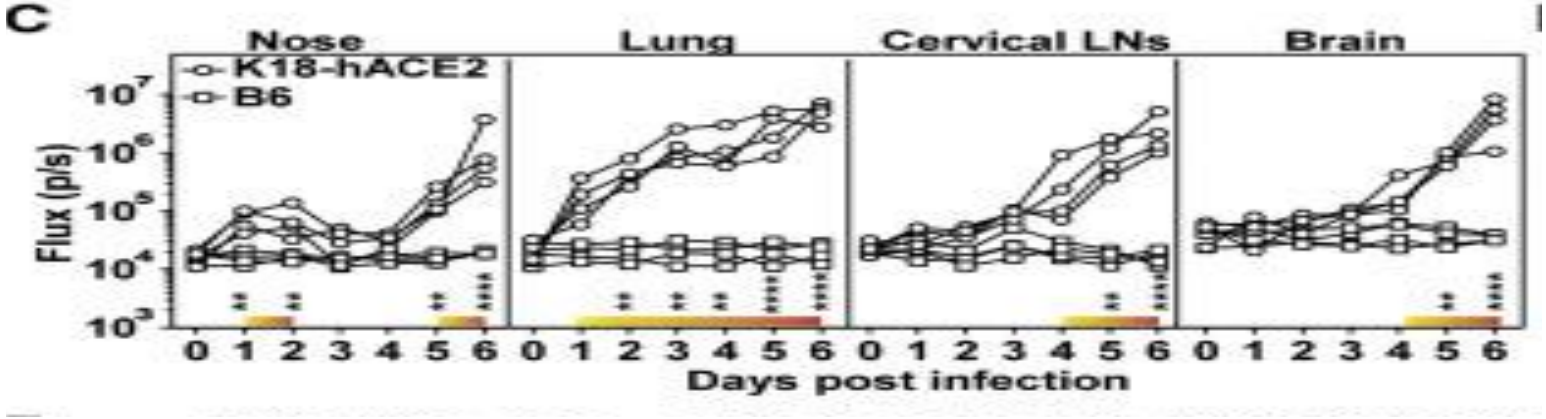

Fig 1 (C)- Temporal quantification of nLuc signal as flux (photons/s) acquired non-invasively in indicated tissues of each animal. The color bar above the x axis (yellow to orange) represents computed signal intensities in K18-hACE2 mice that are statistically significant compared with B6 mice.

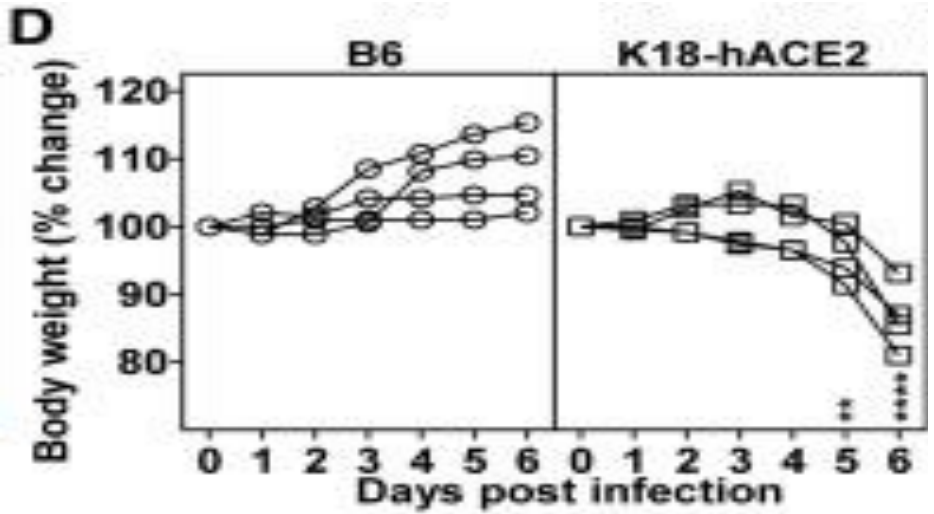

Fig 1(D)- Temporal changes in mouse body weight with initial body weight set to 100% (n = 4 per group)

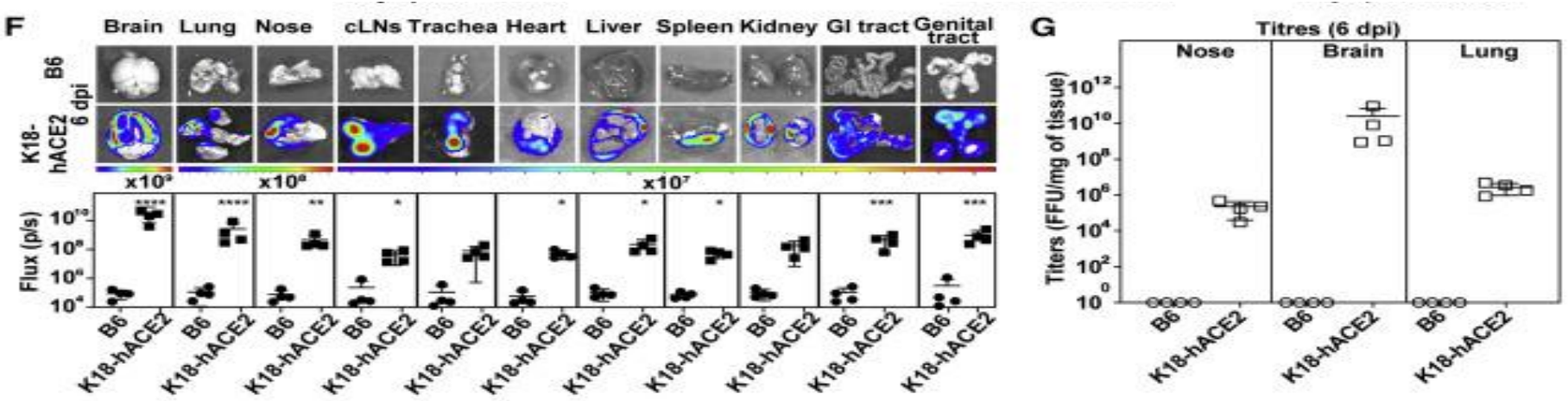

Fig 1 (F)- Ex vivo imaging of indicated organs and quantification of nLuc signal as flux(photons/s) at 6 dpi after necropsy.

Fig 1 (G)- nLuc activity/mg in indicated tissue measured on Vero E6 cells as targets

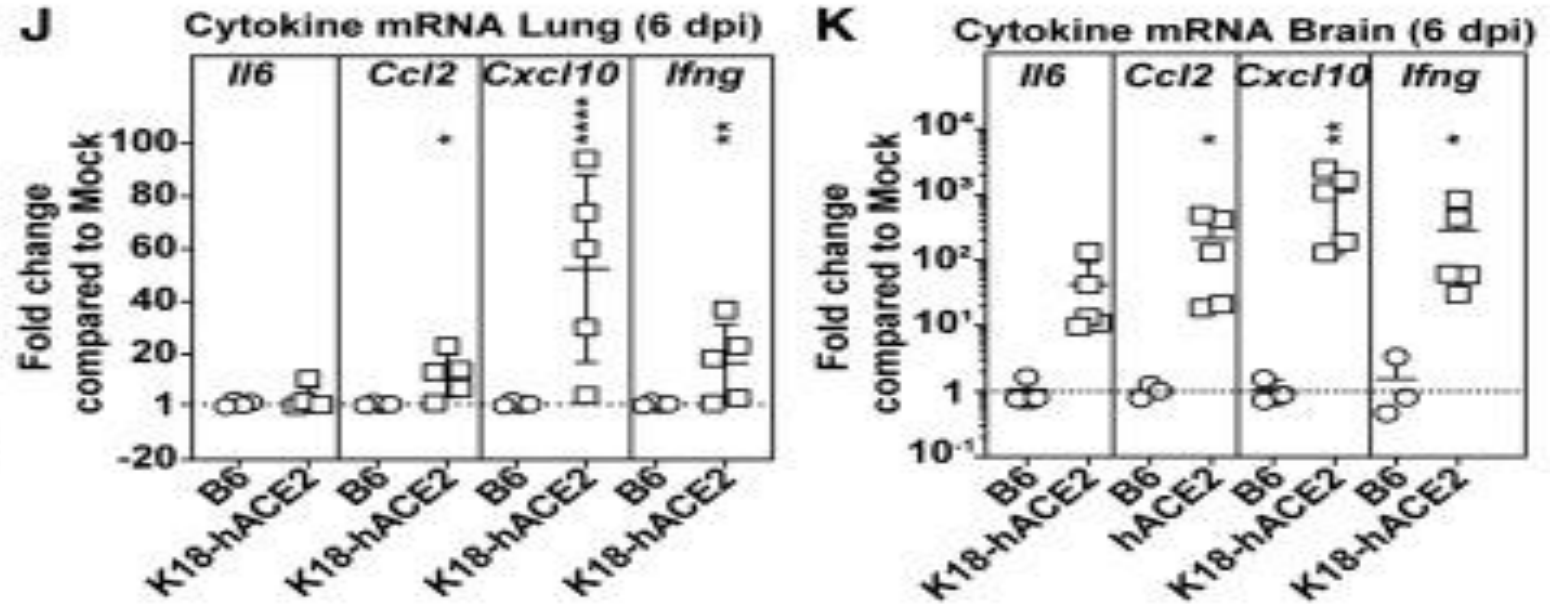

Fig 1 (J and K)- Fold changes in cytokine mRNA expression in lung and brain tissues at 6 dpi. Data were normalized to Gapdh mRNA in the same sample and that in noninfected mice

SARS-CoV-2 virions localize in lung, brain, and testis of infected K18- hACE2 mice

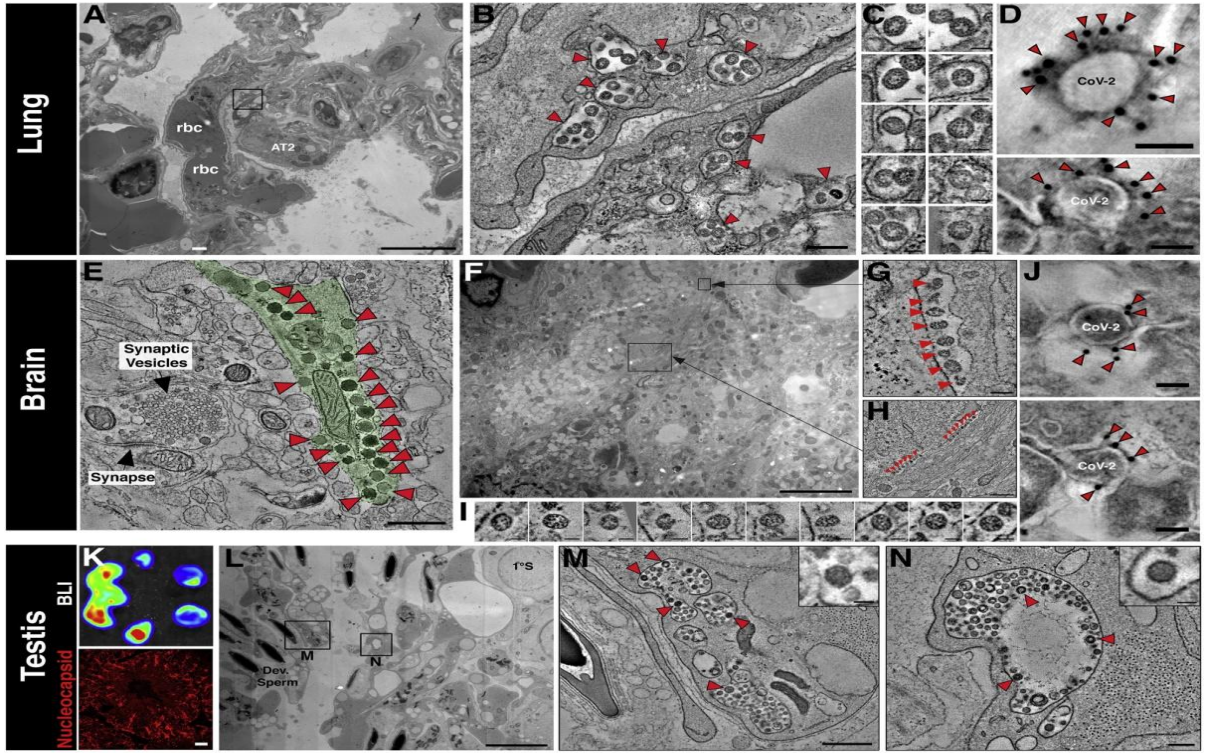

Fig 2 (A- N)

- **SARS-CoV-2 NAbs CV3-1 and CV3-25 from a convalescent donor display highly potent neutralizing activity**

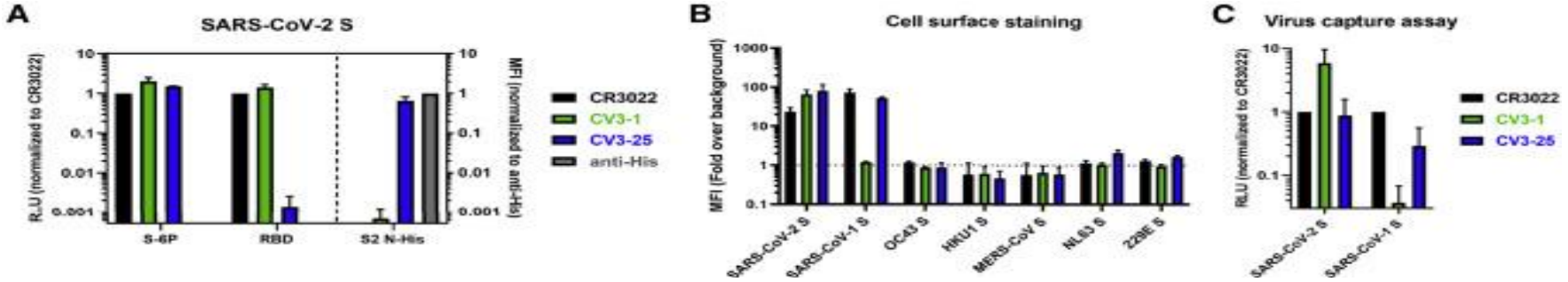

Fig 3 (A) NAb binding to SARS-CoV-2 S ectodomain (S-6P) or RBD estimated by ELISA. NAb binding to SARS-CoV-2 S2 N-His tag protein on cell-surface of transfected 293T cells analyzed by flow cytometry.
(B) Flow cytometric detection of 293T cells expressing S from the indicated human CoVs. MFI from 293T cells transfected with empty vector was used for normalization.
(C) Pseudoviruses bearing SARS-CoV-2 or SARS-CoV-1 S were tested for capture by anti-S NAbs. The cross-reactive CR3022 mAb was used for normalization.

- **SARS-CoV-2 NAbs CV3-1 and CV3-25 from a convalescent donor display highly potent neutralizing activity**

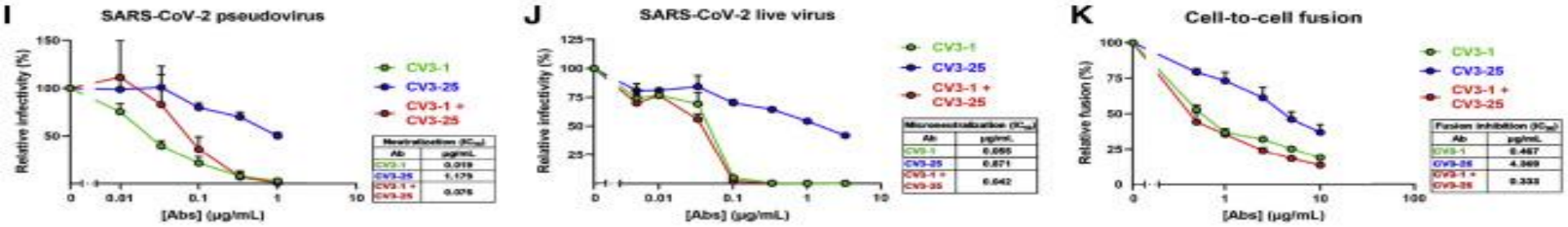

Fig 3 (I)- Neutralizing activity of CV3-1 and CV3-25 alone or in combination (1:1 ratio) on SARS-CoV-2 S bearing pseudoviruses using 293T-ACE2 cells.

(J) Microneutralization activity of anti-S NAbs on live SARS-CoV-2 virus using Vero E6 cells.

(K) Inhibition of cell-to-cell fusion between 293T cells expressing HIV-1 Tat and SARS-CoV-2 S and TZM-bl-ACE2 cells by NAbs. Half maximal inhibitory antibody concentration (IC50) values in (I–K) were determined by normalized non-linear regression analyses.

Evaluate Fc-mediated effector function

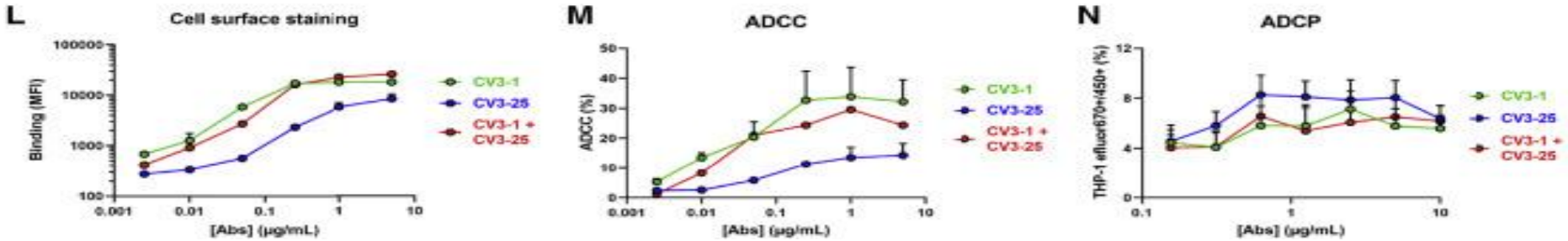

Fig 3 (L)- MFI of CEM.NKr cells expressing SARS-CoV-2 S (CEM.NKr-S) stained with indicated amounts of NAbs and normalized to parental CEM.NKr.
(M) Percentage of ADCC in the presence of titrated amounts of NAbs using 1:1 ratio of parental CEM.NKr cells and CEM.NKr-S cells as targets when PBMCs from non-infected donors were used as effector cells
(N) Percentage of ADCP in the presence of titrated amounts of NAbs using CEM.NKr-S cells as targets and THP-1 cells as phagocytic cells.

Prophylactic treatment with NAbs protects K18-hACE2 mice from SARS-CoV-2 infection

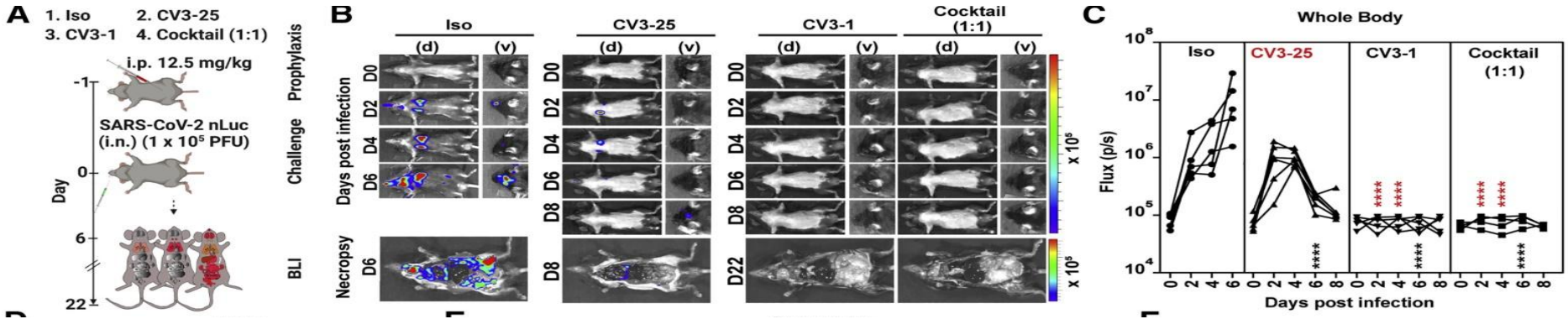

Fig 4 (A)- Experimental design to test in vivo efficacy of NAbs CV3-1 and
(B) Representative BLI images of SARS-CoV-2-nLuc-infected mice
(C)Temporal quantification of nLuc signal as flux (photons/s) computed non-invasively in whole body

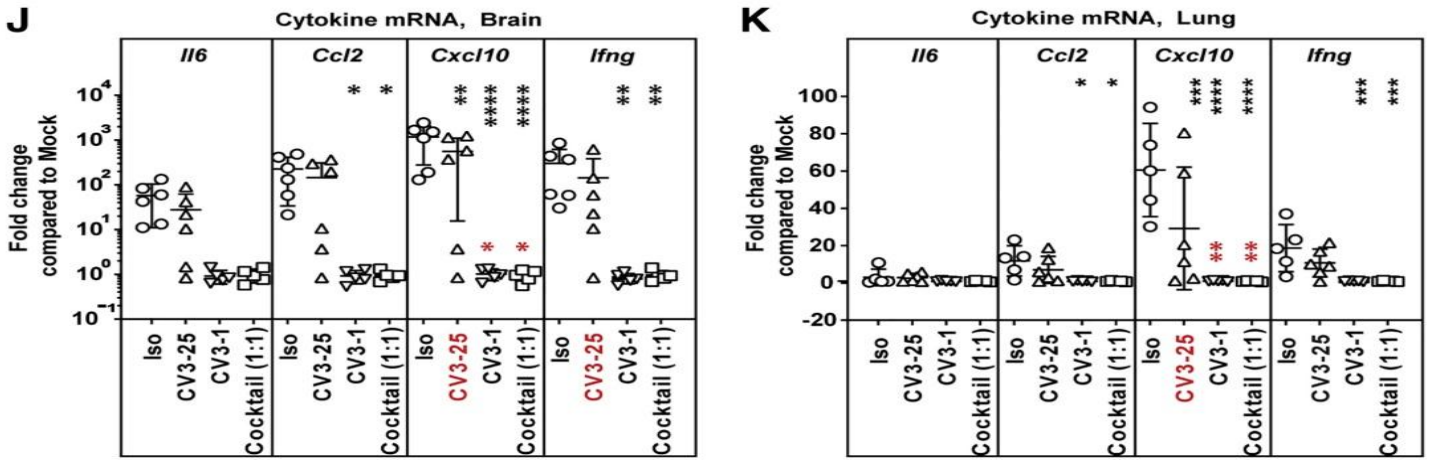

Figure 4- (J and K) Fold changes in cytokine mRNA expression in lung and brain tissues. Data were

normalized to Gapdh mRNA. Viral loads

(I) and inflammatory cytokine profile (J and K) were determined after necropsy for mice that succumbed to infection at 6 dpi and in mice surviving at 22 dpi

CV3-1 and CV3-25 require antibody effector functions for in vivo efficacy

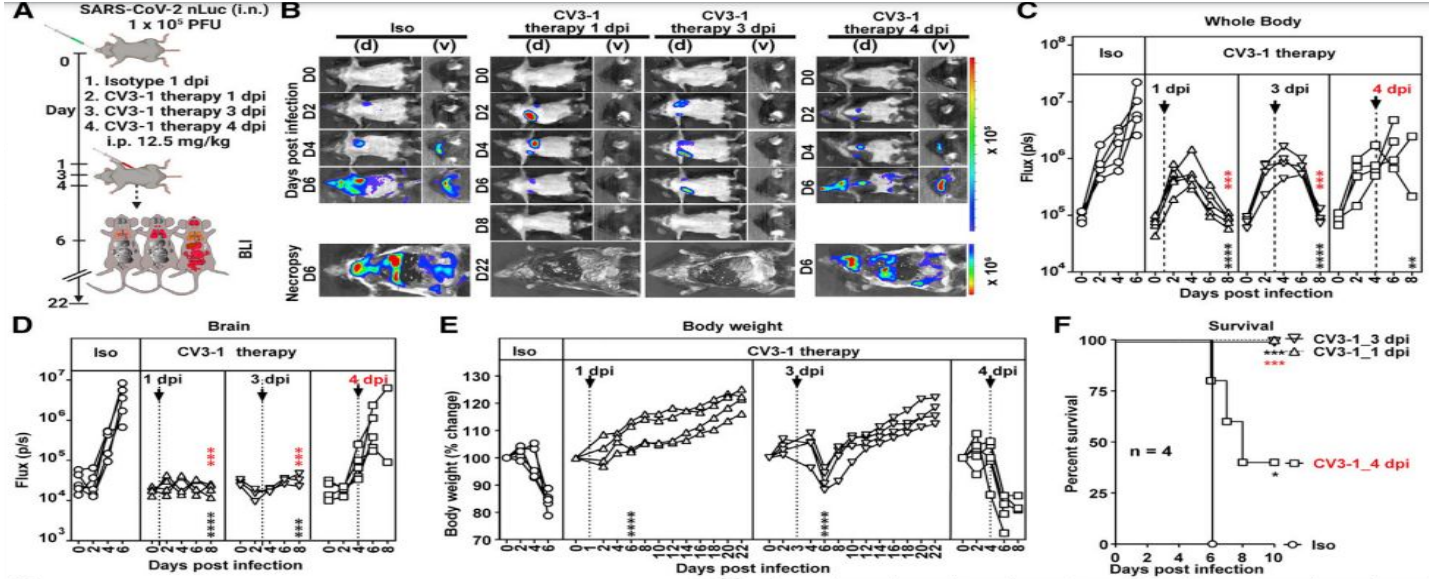

Figure 5-(A)Experimental design to test therapeutic efficacy of NAb CV3-1 and its corresponding leucine to alanine (LALA) mutant administered i.p. (12.5 mg/kg body weight) in K18-hACE2 mice 3 dpi with SARS-CoV-2

A) Representative images from temporal BLI of SARS-CoV-2-nLuc-infected mice

(C) Temporal quantification of nLuc signal as flux computed non-invasively in whole body

(E) Temporal changes in mouse body weight with initial body weight set to 100%.

(F) Kaplan-Meier survival curves of mice statistically compared by log-rank (Mantel-Cox) test

Fc-mediated antibody effector functions contribute to the in vivo efficacy of CV3-1

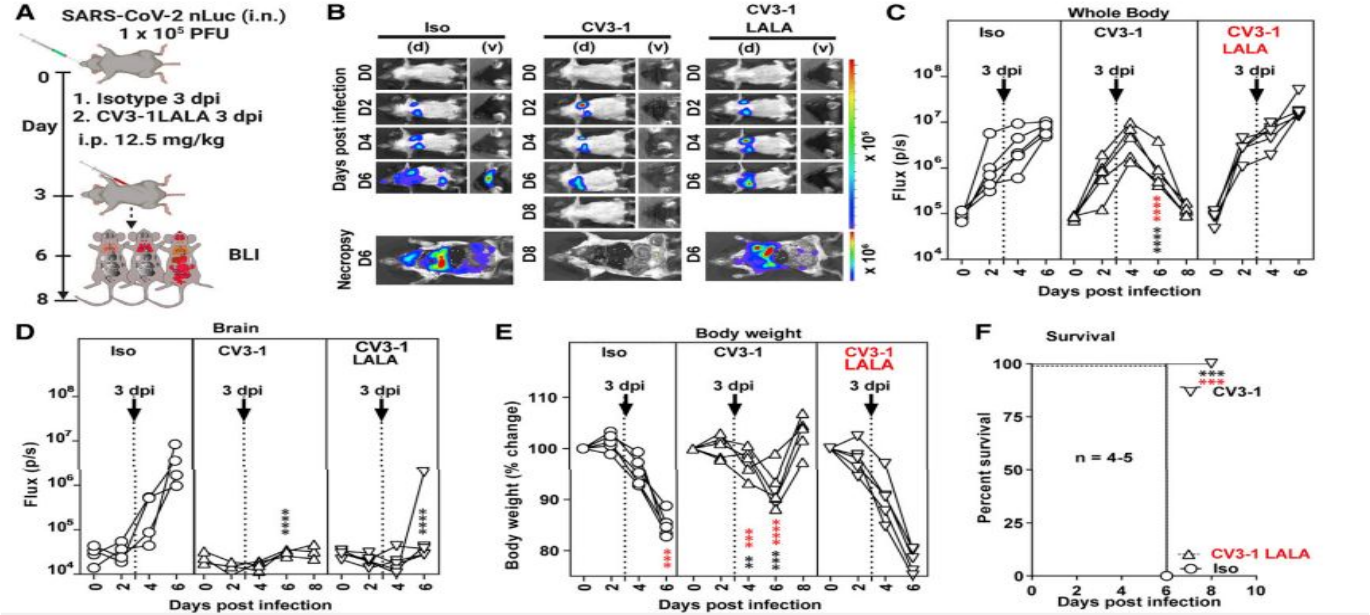

Fig 6 (A) Experimental design to test therapeutic efficacy of NAb CV3-1 and its corresponding leucine to alanine (LALA) mutant

(B) temporal BLI of SARS-CoV-2-nLuc-infected mice in ventral (v) and dorsal (d) positions.

(C and D) quantification of nLuc signal in whole body (C) or brain (D).

(E) Temporal changes in mouse body weight with initial body weight set to 100%. (F) Kaplan-Meier survival curves of mice statistically compared by log-rank (Mantel-Cox) test.

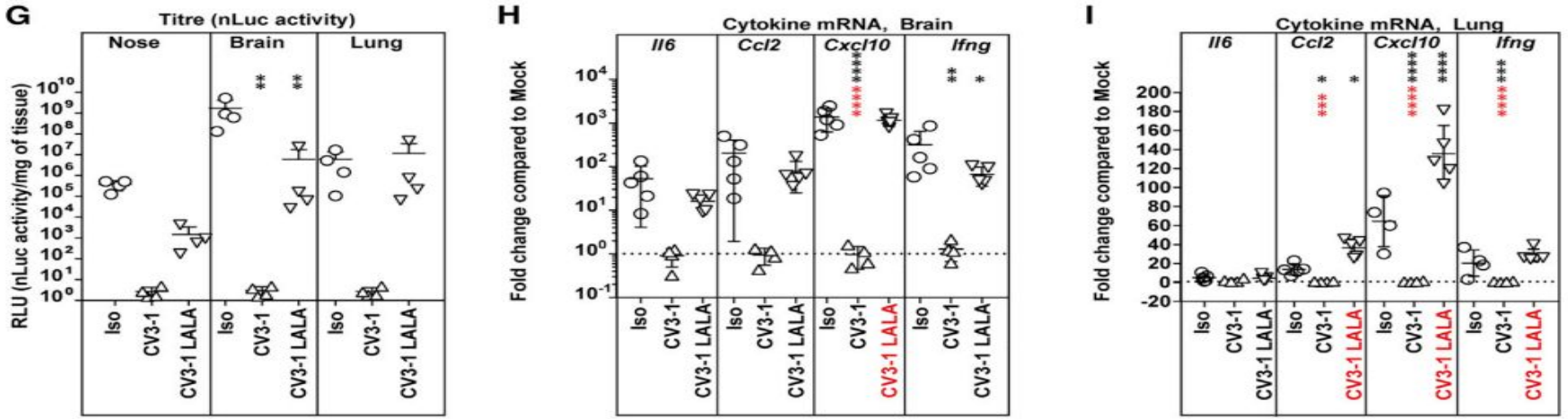

Fig 6 (G- I) Viral loads (nLuc activity/mg tissue) measured in Vero E6 cells as targets. Non-detectable virus amounts were set to 1. (H and I) Fold changes in cytokine mRNA expression in lung and brain tissues. Data were normalized to Gapdh mRNA in the same sample and that in non-infected mice after necropsy.

DISCUSSION

- Dynamics and pathogenesis of SARS-CoV-2 infection in mice investigated by whole-body-imaging approach. BLI revealed:

I. SARS-CoV-2 first replicates in nasal cavity, reaches lungs at 1 dpi and spreading to other organs including brain at 4 dpi.
II. NAbs CV3-1 (targets S RBD) and CV3-25 (binds S2 domain) differed in ability to protect or treat SARS-CoV-2 infection
III. Widespread distribution of NAb within the animals, and persistence for at least a week after
IV. CV3-1 displays one of the most potent in vivo efficacy profiles with a broad therapeutic window till 3 dpi.
V. CV3-25 NAb also conferred protection, albeit not as potently as CV3-1

- Neutralizing capacity of NAbs alone is insufficient to garner clinical protection.
- LALA variants of CV3-1 revealed a crucial role for Fc-mediated interactions in augmenting *in vivo* protection for therapy and prophylaxis
- Diminishing Fc function of CV3-1 completely compromised its ability to therapeutically cure mice.
- Fc region plays an additional protective role in limiting immunopathology by dampening inflammatory responses.
- A previously reported, NAb engaged only monocytes for *in vivo* activity. In contrast, CV3-1 engaged Fc-interacting neutrophils, monocytes, and NK cells for its *in vivo* efficacy. Thus, in addition to potent neutralizing activity, effective engagement of innate immune components contributed to the high *in vivo* potency of CV3-1.

Thanks for your attention